Pergamon

Int. J. Non-Linear Mechanics, Vol. 31, No. 5, pp. 601–617, 1996

0020–7462/96 $15.00 + 0.00

S0020–7462(96)00025-X

SIMULATION OF A CLASS OF NON-NORMAL RANDOM PROCESSES

Kurtis R. Gurley,* Ahsan Kareem and Michael A. Tognarelli

Department of Civil Engineering and Geological Sciences, University of Notre Dame, Notre Dame, IN 46556, U.S.A.

Abstract—This study addresses the simulation of a class of non-normal processes based on measured samples and sample characteristics of the system input and output. The class of non-normal processes considered here concerns environmental loads, such as wind and wave loads, and associated structural responses. First, static transformation techniques are used to perform simulations of the underlying Gaussian time or autocorrelation sample. An optimization procedure is employed to overcome errors associated with a truncated Hermite polynomial transformation. This method is able to produce simulations which closely match the sample process histogram, power spectral density, and central moments through fourth order. However, it does not retain the specific structure of the phase relationship between frequency components, demonstrated by the inability to match higher order spectra. A Volterra series up to second order with analytical kernels is employed to demonstrate the bispectral matching made possible with memory models. A neural network system identification model is employed for simulation of output when measured system input is available, and also demonstrates the ability to match higher order spectral characteristics. Copyright © 1996 Elsevier Science Ltd.

Keywords: non-normal, simulation, random processes, neural networks, higher order statistics, bispectrum wind pressure, ocean waves

INTRODUCTION

The complete analysis of dynamic system reliability necessarily includes a statistical analysis of extreme response. Often, the response of a system under consideration is non-Gaussian due to non-normal input, non-linear system properties, or a combination of both. The presence of non-linearities leads to extreme response statistics that no longer resemble those extreme models based on Gaussian processes. The importance of the extreme response to system reliability has prompted much research in the development of techniques to predict these extreme statistics (e.g. solution strategies for Volterra systems). In order to validate these extreme prediction models, time domain response simulation is attractive, since the equations of motion may be integrated directly to include the full non-linearities. The simulation of Gaussian random processes is well established [1–4]. Progress in the simulation of non-Gaussian processes has been elusive, but necessary for time domain simulation of system response to non-Gaussian input (e.g. large amplitude waves on offshore platforms, and wind pressure fluctuations on cladding components). This work considers several techniques to simulate non-Gaussian stationary random processes concerning wind and wave related processes [5, 6].

The focus in this work is on the transformation of Gaussian simulations to non-normal processes, based on information provided in samples of the desired non-Gaussian process. We concentrate on the class of non-Gaussian processes typical of localized wind pressures as well as that associated with the response of non-linear offshore systems to wind and wave fields. There may exist practical classes of non-Gaussian processes for which the tools presented herein are not necessarily appropriate.

STATIC TRANSFORMATION METHODS

Probability transformation

Static transforms relating a non-Gaussian process with its underlying Gaussian process have been the basis of a variety of non-normal process simulation techniques. A sample of

* Author to whom correspondence should be addressed.

static transformation techniques can be found in refs [7–10]. The few studies in this context have looked at simulation based on a target power spectral density and target probability density function [11, 12]. A summary of several techniques including the use of filtered Poisson δ-correlated processes and α-stable processes is found in a recent book by Grigoriu [13].

An approach used by Yamazaki and Shinozuka [12] begins with the simulation of a Gaussian process $u(t)$ which is then transformed to the desired non-Gaussian process $y(t)$ through the following mapping:

$$y(t) = F_x^{-1}\{\Phi(u)\}. \tag{1}$$

A similar concept utilizing the translation process has been introduced by Grigoriu [7]. Yamazaki and Shinozuka use an iterative procedure to match the desired target spectrum by updating the spectrum of the initial Gaussian process, since the non-linear transformation in eqn (1) also modifies the spectral contents. This iterative procedure does not guarantee convergence for all classes of non-linear processes. For some $y(t)$ there may be no corresponding Gaussian form $u(t)$ with a matching spectrum.

Correlation distortion

The necessity for an iterative procedure may be eliminated if one begins with the target spectrum or autocorrelation of the non-Gaussian process and transforms it to the underlying correlation of the Gaussian process. This approach is referred to as the correlation–distortion method in stochastic systems literature [10, 14, 15]. For a given static single-valued non-linearity $x = g(u)$, where u is a standard normal Gaussian process, the desired autocorrelation of x in terms of y can be expressed as [10]:

$$R_{uu}(\tau) = \sum_{k=0}^{\infty} a_k^2 \rho_{xx}^k(\tau); \qquad a_k = \frac{1}{\sqrt{2\pi k!}} \int_{-\infty}^{\infty} g(\sigma u) \exp\left(-\frac{u^2}{2}\right) H_k(u)\,\mathrm{d}u, \tag{2}$$

where ρ_{xx} is the normalized autocorrelation of the non-Gaussian process, and $H_k(u)$ is the kth Hermite polynomial given by

$$H_k(u) = (-1)^k \exp\left(\frac{u^2}{2}\right) \frac{\mathrm{d}^k}{\mathrm{d}u^k}\left[\exp\left(-\frac{u^2}{2}\right)\right]. \tag{3}$$

An alternative to the preceding approach is to express x as a function of a polynomial whose coefficients are determined by a minimization procedure, e.g. Ammon [11]. Alternatively one may use translational models involving Hermite moment transformation models described earlier. In this study, we utilize a Hermite model for its convenience and availability in the literature. A simulation based on the schematic shown in Fig. 1 would eliminate the spectral distortion caused by the non-linear transformation, since its inverse is employed to reverse the distortion. The simulation algorithm is as follows: (i) estimate the auto-correlation of the mean-removed normalized sample non-Gaussian process to be simulated ($R_{xx}(\tau)$); (ii) transform to the autocorrelation of the underlying Gaussian process ($R_{uu}(\tau)$) by solving for $R_{uu}(\tau)$ [8] in the following equation:

$$R_{xx}(\tau) = \alpha^2[R_{uu}(\tau) + 2\hat{h}_3^2 R_{uu}^2(\tau) + 6\hat{h}_4^2 R_{uu}^3(\tau)], \tag{4}$$

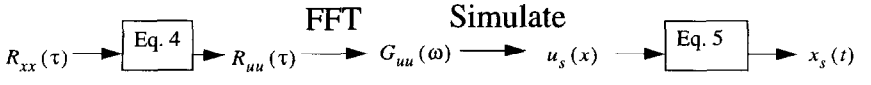

Fig. 1. Schematic of the correlation distortion method.

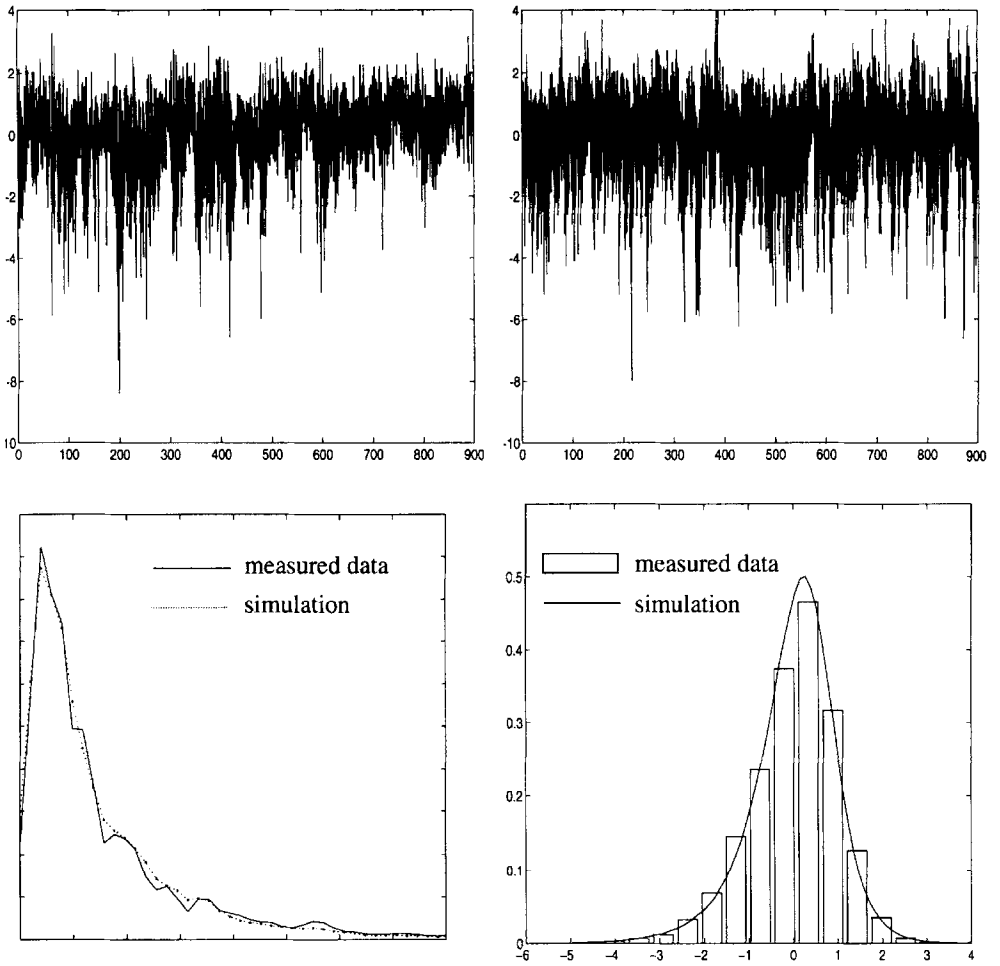

Fig. 2. Measured wind pressure signal (top left), a correlation distortion simulation (top right), and power spectral density and pdf of the measured data and ensemble of 100 simulations.

where

$$\hat{h}_3 = \frac{\gamma_3}{4 + 2\sqrt{1 + 1.5\gamma_4}}, \qquad \hat{h}_4 = \frac{\sqrt{1 + 1.5\gamma_4} - 1}{18}, \qquad \alpha = \frac{1}{\sqrt{1 + 2\hat{h}_3^2 + 6\hat{h}_4^2}},$$

and γ_3 and γ_4 are the skewness and kurtosis of the fluctuating process; (iii) simulate a Gaussian process using the spectrum, $G_{uu}(\omega)$, associated with $R_{uu}(\tau)$; (iv) transform this simulated process u_s back to a non-Gaussian process using

$$x = \alpha[u + \hat{h}_3(u^2 - 1) + \hat{h}_4(u^3 - 3u)]; \tag{5}$$

(v) replace the mean and variance of the original parent process to produce a simulation, x_s of the original non-Gaussian process x.

Figure 2 compares a measured wind pressure signal with a single realization of a correlation distortion simulation of that signal in the top left and right figures, respectively. Note the undesirable positive extreme behavior in the simulation that is not seen in the sample. The bottom figures compare the power spectral density and PDF of the measured data with that from the ensemble average of 100 correlation distortion simulations. The statistical moments of the standardized original signal are compared with the average moment statistics of the 100 realizations in Table 1. The higher positive kurtosis in the simulations can be observed in both the time history and the PDF comparison. Unless otherwise noted, the comparison of the statistical properties of the simulation with those of the sample process is made using an ensemble of 100 realizations for the sake of expedience. Ensembles

Table 1. Statistics of measured wind pressure data and ensemble averaged simulated data

	Standard deviation	Coefficient of skewness	Coefficient of kurtosis
Measured wind data	1.0	−0.8309	4.9940
Ensemble of 100 correlation distortion simulations	0.9927	−0.7960	5.6711
Ensemble of 100 modified direct transformation simulations	0.9960	−0.8120	4.7676

of up to 1000 were used in the initial phases of this work, and showed little difference in the results. A later example using 2000 realizations will be shown to add nothing to the qualitative conclusions based on 100 realizations.

There are several restrictions on the application of the correlation distortion method. The static transformation suggested in equation (4) is appropriate for processes in which the non-Gaussian behavior can be adequately limited to a non-zero skewness and a kurtosis not equal to three. For processes for which moments beyond fourth order are necessary to adequately describe the non-Gaussian behavior, the method loses accuracy, as this higher order information is distorted through the inverse and forward transformations. Further, the solution of equation (4) for $R_{uu}(\tau)$ is not guaranteed to be positive definite for all $R_{xx}(\tau)$.

Direct transformation

An alternative to the correlation-based approach is to begin with a sample of a non-Gaussian time history rather than its autocorrelation. The schematic in Fig. 3 then provides simulations of the sample process. The non-Gaussian sample process, $x(t)$, is transformed to its Gaussian underlying form, $u(x)$, through

$$u(x) = [\sqrt{\xi^2(x) + c} + \xi(x)]^{1/3} - [\sqrt{\xi^2(x) + c} - \xi(x)]^{1/3} - a,$$

where

$$\xi(x) = 1.5b\left(a + \frac{x}{\alpha}\right) - a^3, \qquad a = \frac{\hat{h}_3}{3\hat{h}_4}, \qquad b = \frac{1}{3\hat{h}_4}, \qquad c = (b - 1 - a^2)^3, \tag{6}$$

and the other parameters are defined after equation (4). Subsequently, linear simulations created through standard techniques based on the target spectrum of the Gaussian process, $G_{uu}(\omega)$, are transformed back to the non-Gaussian parent form through eqn (5).

The shortcoming of this direct transformation technique is that the simulated non-Gaussian signal power spectrum does not match the sample non-Gaussian spectrum to a satisfactory degree for the example sample processes we have used in subsequent examples. This distortion may stem from the inability of the truncated Hermite moment transformation in eqn (6) to produce a Gaussian signal for cases when the parent signal is highly non-Gaussian. Specifically, non-Gaussian behavior requiring moments beyond fourth order for characterization are not addressed, and their presence distorts the static transformation from non-Gaussian to Gaussian. The linear simulation is then based on a target spectrum derived from a process which is assumed Gaussian, but is not. It is at this point, indicated in Fig. 3 by the dashed box, where the frequency information is distorted, and results in poor simulations. One option for improving results is to add terms to the Hermite series until a Gaussian transformation is achieved. This may require a different number of terms to achieve accuracy for varying input sample signals, and leads to a very complex solution for $u(x)$ in the higher order equivalent of equation (6).

An example of the potential for distortion using the direct transformation method is seen in Fig. 4. The top figures compare the same measured wind pressure signal seen in Fig. 2 with a direct transformation simulation of the signal. The power spectral density and PDF

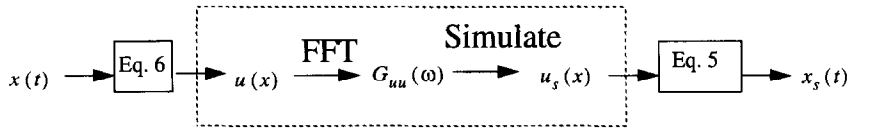

Fig. 3. Schematic of the direct transformation method.

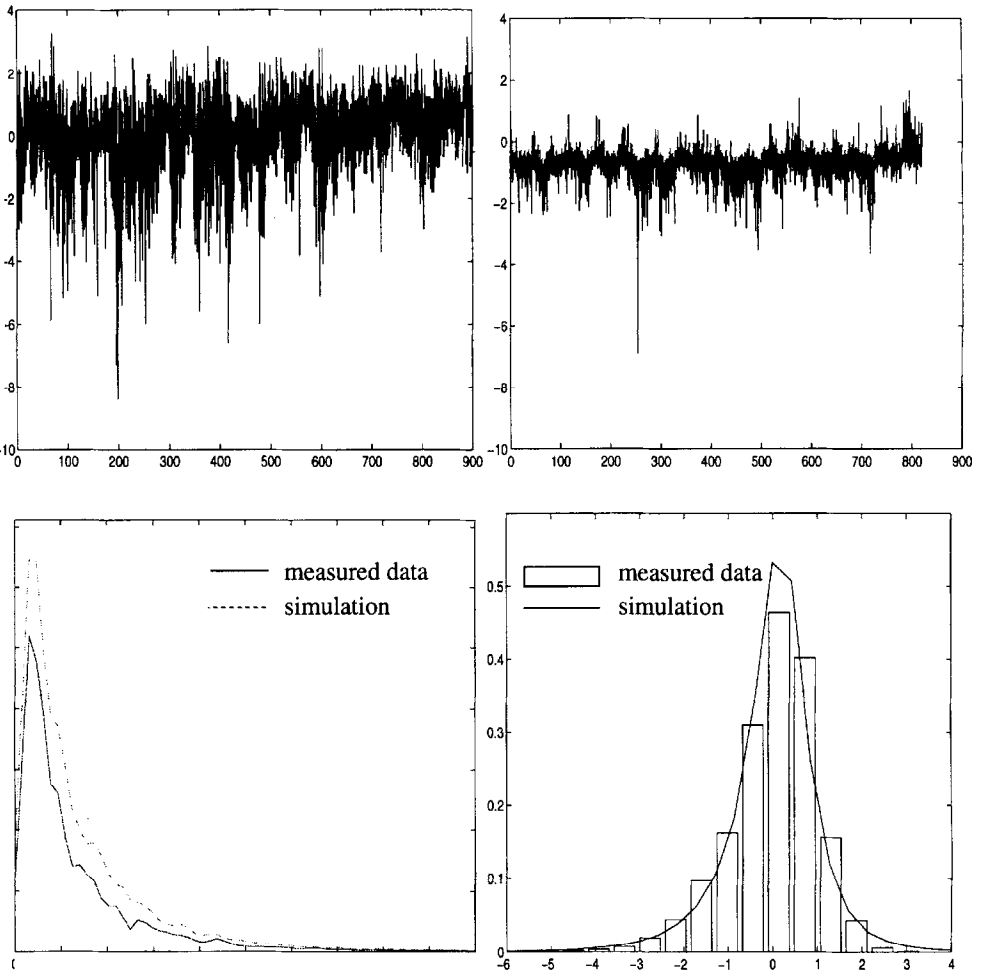

Fig. 4. Measured wind pressure signal (top left), a direct transformation simulation (top right), and power spectral density and pdf of the measured data and ensemble of 100 simulations.

of the measured data are compared with an ensemble of 100 realizations in the lower figures and show poor agreement. Clearly, this method is not applicable to this sample process.

Modified direct transformation

A modification is now suggested, shown in Fig. 5, to remove this distortion in the direct transformation method. Referring to equation (6), it can be seen that the governing parameters $\hat{h}_3$, $\hat{h}_4$, a, b, c, α, and thus $u(x)$, are dependent on the skewness and kurtosis, γ_3 and γ_4. Since it is required that the process, $u(x)$, be Gaussian in order to avoid the distortion effects discussed above, γ_3 and γ_4 may be treated as adjustable input parameters in order to force the transformed process, $u(x)$, to be Gaussian in terms of the third and fourth moments. Optimization of these two parameters is based on the minimization of the function

$$\min(\gamma_{4_u}^2 + \gamma_{3_u}^2), \tag{7}$$

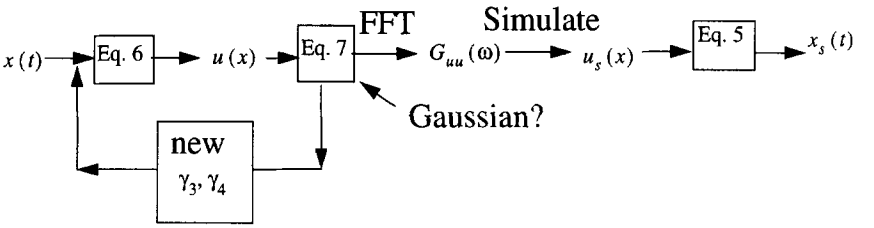

Fig. 5. Schematic of the modified direct transformation method.

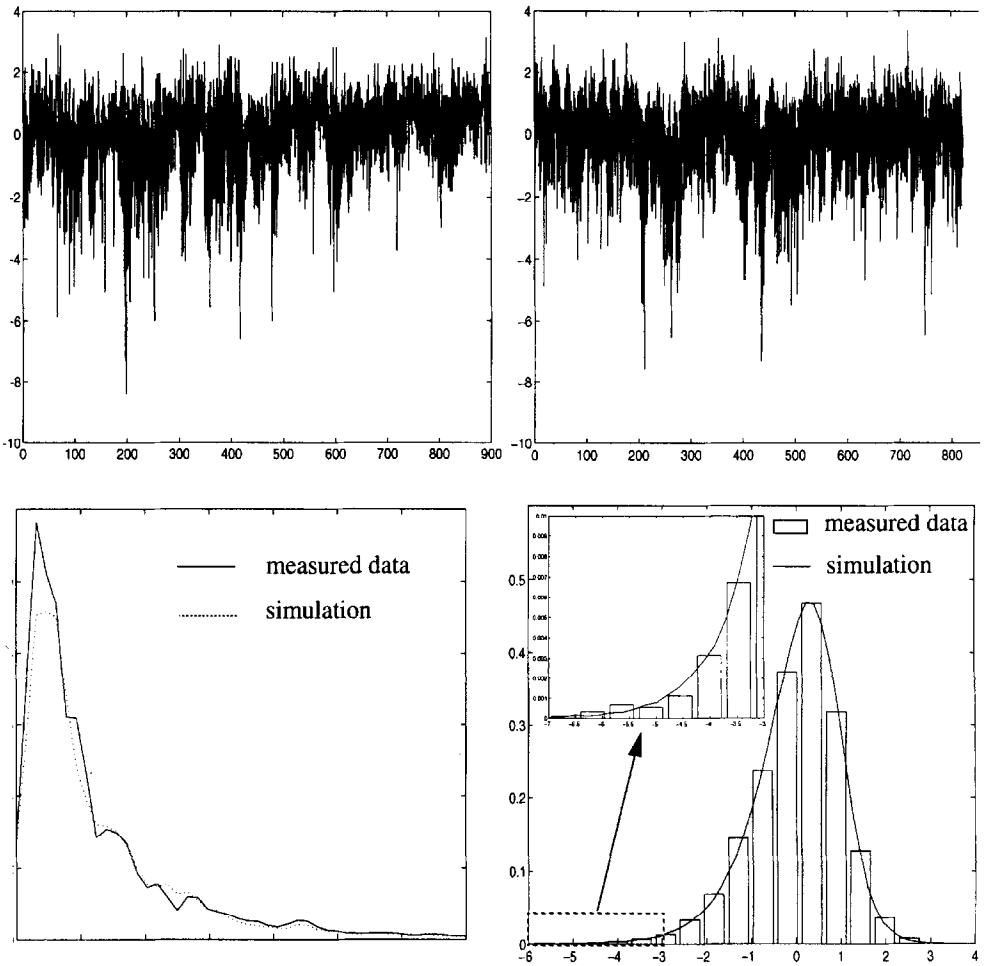

Fig. 6. Measured wind pressure signal (top left), a direct transformation simulation (top right), and power spectral density and pdf of the measured data and ensemble of 100 simulations.

where γ_{3_u}, γ_{4_u} are the skewness and kurtosis of the transformed process $u(x)$. The optimized input parameters γ_3 and γ_4 now provide a Gaussian process in terms of third and fourth moments, and the linear simulations do not contain distortion of the frequency content. The same parameters are used to transform back to a non-Gaussian simulation whose PDF and power spectral density closely match those of the sample process. This correction is essentially a quantification of the error in truncating the Hermite series after the third term.

An example of the improvement afforded by the modified direct transformation method is demonstrated in Fig. 6. Again the measured pressure trace in the top left is simulated and displayed in the top right. The power spectral density and PDF of the data and simulations are shown in the bottom figures. Table 1 shows an improved ability to match higher order statistics compared with the correlation distortion method. By observing the positive and

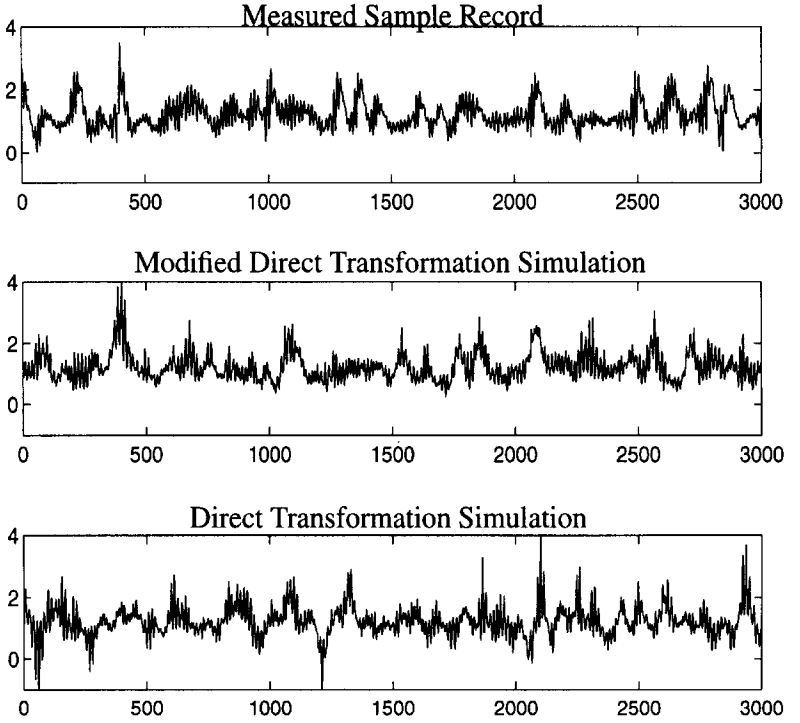

Fig. 7. Measured TLP response, modified direct transformation and direct transformation simulations.

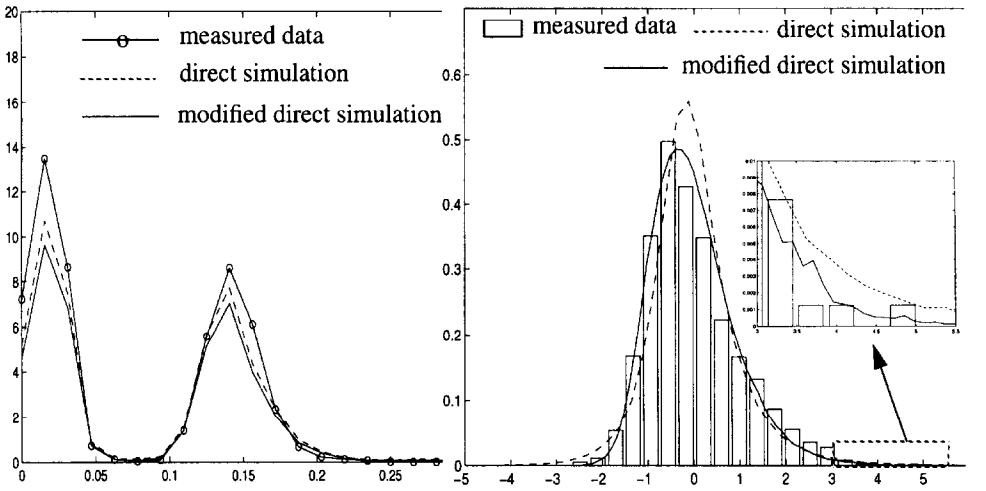

Fig. 8. Power spectral density and pdf of measured TLP response signal and ensemble of 2000 realizations.

negative extreme behavior, as well as fluctuation amplitude close to the mean, the modified direct simulation can be seen to emulate the characteristics of the measured process better than correlation distortion. This behavior is quantified by the kurtosis and standard deviation, which match well with the data (Table 1).

A second example further demonstrates the performance of the modified direct transformation. In this case the sample process to be simulated is the measured response of a model tension leg platform (TLP) under a random wind and wave field in a test facility. The response is highly non-Gaussian and has two dominant frequencies. Figure 7 shows a portion of the sample measurement, a simulation using modified direct transformation, and a direct transformation simulation in the top, middle, and bottom plots, respectively. Figure 8 is a comparison of the PDF and power spectral density of the sample and 2000

Table 2. Statistics of measured TLP response data and ensemble averaged simulated data, # = 100 realizations, and (#) = 2000 realizations

	Standard deviation	Coefficient of skewness	Coefficient of kurtosis
Measured TLP data	1.0	0.8165	3.7455
Ensemble of 100 and (2000) modified direct simulations	0.9720 (0.9690)	0.8187 (0.8298)	4.2127 (4.2650)
Ensemble of 100 and (2000) direct transformation simulations	0.9633 (0.9672)	0.8419 (0.7546)	7.4672 (7.1469)

realizations of the simulations. Table 2 lists statistics from the data, an ensemble of 100 realizations, and an ensemble of 2000 realizations in parentheses. The direct transformation provides simulations whose skewness characteristics adequately match the sample (Table 2). However, large negative excursions in the realization are not observed in the sample, and lead to a significantly higher kurtosis (Table 2), as well as a poor fit of the PDF to the data, most importantly in the negative tail region. The modified direct transformation provides realizations which match the sample PDF well, particularly in terms of positive and negative extreme behavior.

The modified direct transformation method, for the two sample processes considered, is able to provide simulations which match the PDF and power spectral density of the sample process, and match the scalar representations of higher order statistics (skewness and kurtosis) through fourth order. Later, an example will be presented where these comparisons are not as favorable.

The shortcoming of any static transformation is its inability to retain the phase interaction among related frequency components. The bispectrum is a representation of the quadratically phase coupled frequency components. Just as the power spectral density is the distribution of the variance of a signal with respect to frequency, the bispectrum is the distribution of skewness with respect to frequency pairs. Although the modified direct transformation is able to replicate the volume under the bispectrum, i.e. the skewness, it is not able to correctly match the distribution of skewness with respect to frequency. Figure 9 compares the bispectrum contour of the sample TLP response process with that of the direct and modified direct transformations. Neither simulation is able to adequately match the shape of the sample bispectrum. The non-linear processes considered in this study can be described by a quadratic form [6, 16, 17]. Although higher-order spectra beyond the bispectrum may be calculated, it is only necessary to show the existence of the bispectrum to demonstrate the non-Gaussian behavior of quadratic processes.

When the only available information is a sample of the final process to be simulated (e.g. wind pressure on a building face), this static transformation method is quick and promising. However, if more information is available (e.g. the upwind wind velocity), it is possible to better simulate the desired process by establishing a system identification model between, in this case, velocity and pressure. The limitation of static transformation techniques is overcome by the application of memory-based system identification models.

TRANSFORMATIONS WITH MEMORY

When input and output are available, the non-linear relationship between current time output and previous time input and output may be modeled through a variety of system identification techniques. A model that relates Gaussian input to non-Gaussian output may easily be applied to the simulation of the output process by passing simulations of the Gaussian input through the model. The important phase characteristics of the output are then retained in the simulation through the memory transformation, assuming the model is accurate. Here we consider the application of a Volterra series formulation for polynomial non-linear systems, as well as the empirical development of discrete non-linear differential models through NARMAX (non-linear autoregressive moving average models with exogenous inputs) and neural network models. Examples are provided using a two-term Volterra series with analytical kernels, and an empirical neural network model.

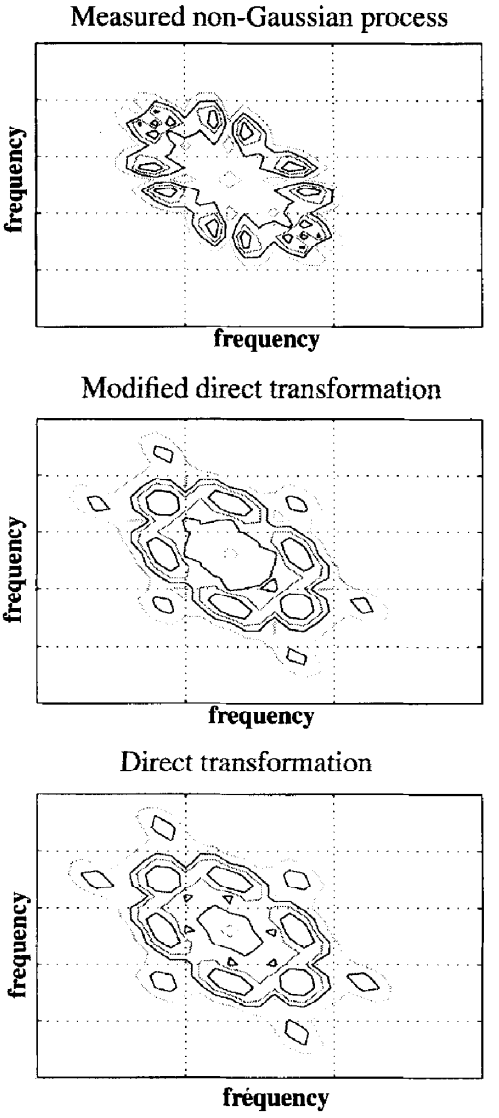

Fig. 9. Contours of the bispectrum of the measured TLP response and the bispectrum of an ensemble of 2000 simulations using the modified direct, and the direct transformation methods.

System identification models for non-Gaussian input and non-Gaussian output are readily available, but are not easily adaptable for simulation purposes. We wish to use transformations to relate easily attained Gaussian simulations to the desired non-Gaussian process. The inability to easily simulate non-Gaussian system input is addressed by the hybrid application of a static transformation in combination with a neural network.

Volterra series model

In the Volterra series formulation, the input–output relationship may be expressed in terms of a hierarchy of linear, quadratic and higher-order transfer functions or impulse response functions [17–19]. These transfer functions can be determined from experimental data or from theoretical considerations. For example, a non-linear system modeled by Volterra's stochastic series expansion is described by

$$y(t) = \int h_1(\tau)x(t-\tau)\,d\tau + \iint h_2(\tau_1, \tau_2)x(t-\tau_1)x(t-\tau_2)\,d\tau_1\,d\tau_2 + \iiint h_3(\tau_1, \tau_2, \tau_3)x(t-\tau_1)x(t-\tau_2)x(t-\tau_3)\,d\tau_1\,d\tau_2\,d\tau_3 + \cdots, \quad (8)$$

where $h_1(\tau)$, $h_2(\tau_1, \tau_2)$ and $h_3(\tau_1, \tau_2, \tau_3)$ are the first, second and third-order impulse response functions.

The Fourier transform of the Volterra series expansion in equation (8) gives the response in the frequency domain as

$$Y(f_i) = H_1(f_i)X(f_i) + \sum_{f_1+f_2=f_i} H_2(f_1,f_2)X(f_1)X(f_2) + \sum_{f_1+f_2+f_3=f_i} H_3(f_1,f_2,f_3)X(f_1)X(f_2)X(f_3) + \cdots \quad (9)$$

The Volterra series model in the frequency domain [equation (9)] lends itself to the simulation of non-linear processes for which the Volterra kernels are available or may be estimated. A non-Gaussian signal resulting from a quadratic transformation of a Gaussian process may be simulated by the addition of second-order contributions to the complex spectral amplitude components at the appropriate sum and difference frequencies before inverse Fourier transforming the sequence to the time domain. These second-order contributions are formed from the products of pairs of linear Fourier components with the quadratic transfer function (QTF) in the frequency domain, and correlate the phase between various frequency components to a degree weighted by the QTF. The memory retained by convolution with the QTF facilitates the simulation of processes that are able to match not only the power spectrum and PDF of the parent process, but the bispectrum as well, e.g. Peinelt and Bucher [20].

The estimation of the higher-order transfer functions in equation (9) requires the calculation of the cross-bispectrum and cross-trispectrum of the input and output processes. As examples of the utility of bispectra and trispectra in frequency domain analyses, consider two types of non-linear functions of a zero-mean, Gaussian random process, $u(t)$. Functions, $g(u(t))$, for which all odd-order moments vanish, will be considered statistically symmetric non-linearities, while those for which, in general, all moments are non-zero will be considered statistically asymmetric non-linearities. For instance, $g(u(t)) = u^3(t)$ is a statistically symmetric non-linearity, whereas $g(u(t)) = u^2(t)$ is statistically asymmetric. In the statistical characterization of the statistically asymmetric non-linearity, we expect non-Gaussianity in the form of non-zero skewness, which we can characterize in terms of frequency pairs via the bispectrum. Indeed, for some cases, we can successfully employ a technique known as equivalent statistical quadratization, which retains memory by employing a Volterra series approach in the frequency domain, to approximate a more complicated statistically asymmetric non-linearity as a quadratic polynomial for the determination of higher-order statistics [18, 21]. On the other hand, for the case of a statistically symmetric non-linearity, we expect the skewness to vanish and with it, the bispectrum. Hence, we must turn to the trispectrum, the tri-variate frequency domain representation of the kurtosis, to gain any higher-order statistical information about the non-linear process. While the trispectrum would supplement the statistical evidence of the non-Gaussianity of an asymmetric non-linearity, it is not necessary in such a case as it is in the case of a symmetric non-linearity. Again, under certain circumstances, we may approximate more complex symmetric non-linearities in polynomial forms containing only linear and cubic terms via equivalent statistical cubicization. Implementing the Volterra framework as described above, we can approximate higher-order statistics in situations involving symmetric non-linearities as well.

When the input $x(n)$ and output $y(n)$ of a system is available, the information can be used to estimate the Volterra kernels in equation (9) directly. The first and second order transfer functions are given by

$$H_1(f_i) = \frac{\langle Y(f_i)X^*(f_i)\rangle}{\langle |X(f_i)|^2\rangle} \quad (10)$$

and

$$H_2(f_1,f_2) = \frac{1}{2}\frac{\langle X^*(f_1)X^*(f_2)Y(f_1+f_2)\rangle}{\langle |X(f_1)X(f_2)|^2\rangle}, \quad (11)$$

where $\langle\ \rangle$ is the expected value operator. Equation (9) is then applied to simulate $y(n)$ based on linear simulations of $x(n)$. The formulation for the QTF given in equation (11) is under the assumption of a Gaussian input process $X(f)$. The linear and quadratic transfer functions can also be estimated for a general random input, i.e. without assuming particular statistics of the input [23–25]. For systems where the governing differential equation is known, several methods of analytically approximating the Volterra kernels are available, including variational expansion, harmonic probing, and successive approximation [26].

Conceptually the Volterra series may easily be extended to the simulation of non-linear processes beyond second order [equation (9)], although considerable computation time is added by convolution of the Fourier components with transfer functions beyond quadratic. Also, the acquisition of higher-order transfer functions from measured data becomes difficult and the number of parameters necessary to describe them becomes prohibitive.

NARMAX model

When the system is not yet described, system identification techniques may be used to approximate the Volterra kernels directly, or to develop a discrete governing differential equation. For the latter, NARMAX model algorithms have been developed to identify non-linear systems [27]. The Volterra kernels may then be developed from the parametric NARMAX model through harmonic probing, etc. [24].

The discrete differential equation provided by the NARMAX model may be used as the stand-alone representation of the system. Convenient algorithms are available that use input/output data to define a polynomial model. These algorithms identify the relevant terms in an initial model consisting of all possible combinations of input, output, and noise terms up to a user-specified polynomial order and maximum lag. For example, a model specified as second-order with two delays begins as

$$y(n) = f(y(n-1),\ y(n-2),\ x(n-1),\ x(n-2),\ e(n-1),\ e(n-2)), \tag{12}$$

where $f(\ )$ is the sum of all first and second order combinations of the arguments.

Discussions on NARMAX theory are available in the literature, and a sampling of practical and efficient algorithms may be found in Chen *et al.* [28], and Billings and Tsang [24]. NARMAX provides a more flexible representation of a non-linear system, and generally requires fewer parameters than a Volterra model.

Neural network model

Another recently developed approach to non-linear system identification is the application of neural networks. A multi-layered set of processing elements receives input information and uses the desired final output information to adjust a weighting factor between each of the elements. Figure 10 shows such a network with three weighting layers $W_{ij}(m)$, $m = 1 \ldots 3$, where $i = 1 \ldots N_m$, $j = 1 \ldots N_{m-1}$, and N_m and N_{m-1} are the number of elements in the mth and the $m-1$th layers, respectively. The network in Fig. 10 has two hidden element layers $a_i(1)$ and $a_i(2)$ between the input and output layers $a_i(0)$ and $a_i(3)$. In this example the input layer consists of the input occurring at the same time as the current output from $a_1(3)$, and the two inputs preceding this lead input (a two delay input system). $W_{ij}(m)$ then represents the weighting of the output from the element $a_j(m-1)$ before its input to element $a_i(m)$. The output of each element is a non-linear function of the weighted linear sum of the output from each of the elements in the previous layer as in Kung [29]:

$$b_i(m) = \sum_{j=1}^{N_{m-1}} W_{ij}(m) a_j(m-1) + \theta_i(m); \tag{13}$$

$$a_i(m) = f(b_i(m)) \quad 1 \leqslant i \leqslant N_m; \quad 1 \leqslant m \leqslant 3, \tag{14}$$

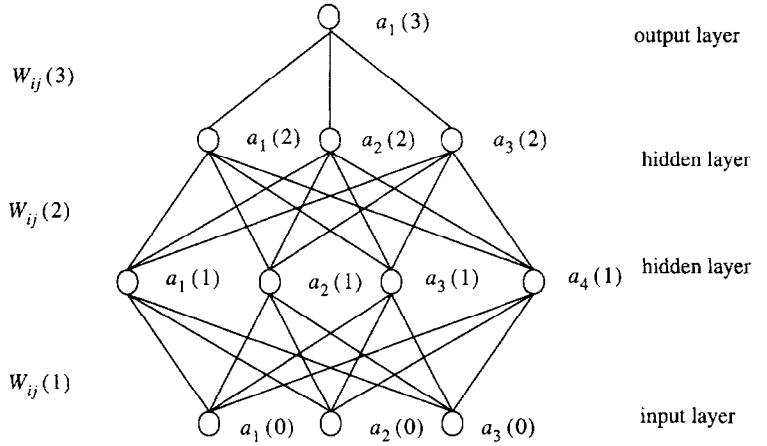

Fig. 10. Multilayer neural network with three weighting layers and two hidden layers (adapted from Kung [29]).

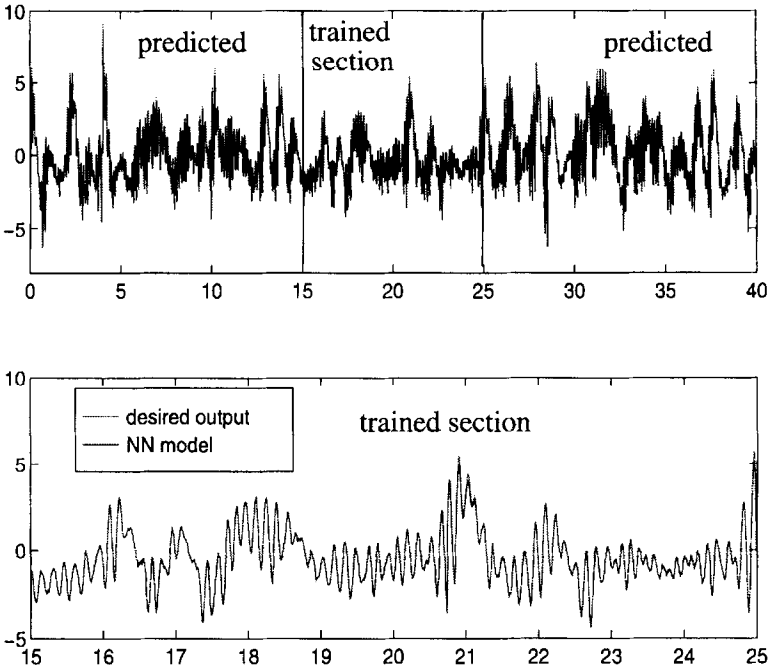

Fig. 11. Measured TLP response signal, trained and predicted neural network output, and a close up of the training section.

where $\theta_i(m)$ is a threshold value fixed for each $a_i(m)$. Various non-linear functions may be applied at the elements, under the restriction that the output must be limited to $0 \leqslant f(b_i) \leqslant 1$. One commonly applied function is the sigmoid function:

$$f(b_i) = \frac{1}{1 + e^{-b_i/\sigma}}, \tag{15}$$

where σ is a parameter to control the shape of $f(b_i)$.

The element weights in the neural network are adjusted iteratively, commonly with a back propagation scheme, which minimizes the error between the resulting and desired final output. This is known as the training phase, in which the optimum model parameters $W_{ij}(m)$, $m = 1 \ldots M$ are identified, where M is the number of network layers, and $M = 3$ for the example in Fig. 10 [29].

An example of the development of a neural network is shown in Fig. 11. The measured TLP response data in Fig. 7 is used as the input to a non-linear difference equation, and

a neural network is used to identify this input/output system. The neural network was trained on a 10 s span of input/output from 15 to 25 s as identified in the top figure, and shown alone in the bottom figure in Fig. 11. The actual desired system output and the neural network estimate are both in the figures, and coincide almost exactly. The entire 40 s input record is then passed through the model, and is shown in the top figure to predict the actual output from the non-linear difference equation extremely well. This accurate prediction capability will be used later for simulation purposes.

Applications

When the convenience of having measured input and output is available, the Volterra, NARMAX and neural network models discussed in the previous section may be used as simulation tools when the input is Gaussian. The input is simulated and passed through the prediction model to produce a non-Gaussian simulation. This technique is much more time consuming than simply applying a static transformation technique to the output alone, but has the advantage of memory built into the model.

A sample of a non-linear simulation using a Volterra series model is shown in Fig. 12. This realization is the surface elevation of gravity waves, with the non-Gaussian train showing the characteristic high peaks and shallow troughs. In this case the second-order Volterra kernel is analytically derived [30–33] and referred to as a non-linear interaction matrix (NIM). The NIM relates a quadratic non-Gaussian process to its underlying Gaussian process. In terms of equation (9), $Y(f)$ is the desired non-Gaussian wave elevation, $X(f)$ is the underlying linear sea state, and $H_1(f)$ is unity. $X(f)$ is first simulated, then used to generate the second-order contributions. The matching of the realizations with the desired target QTF is shown in Fig. 13, where the recovered QTF is an ensemble of 1000 realizations.

A non-linear transformation of Gaussian wave elevation is used for a neural network example. The system input is a linear wave train simulated based on a JONSWAP spectrum with a peakedness of 5, and a peak frequency of 0.05 Hz. The non-linear output, $F(n)$, is generated from the linear wave train, $\eta(n)$, by a generic non-linear function:

$$F(n) = 0.1\eta(n-2) + 0.4\eta^2(n-2) + 0.1\eta(n-1) + 0.5\eta^2(n-1) + 0.2\eta(n) + 0.6\eta^2(n). \tag{16}$$

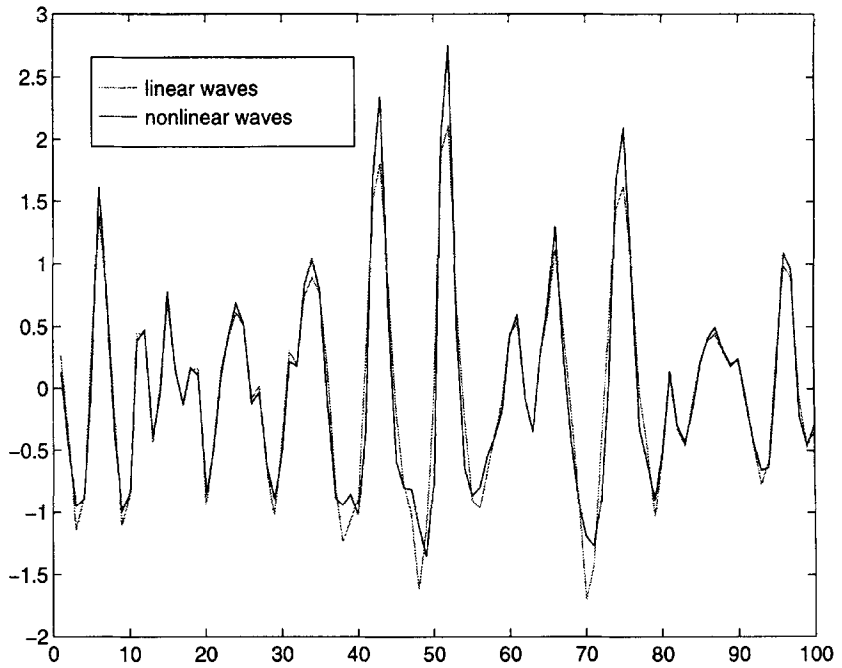

Fig. 12. Realization of a Gaussian and non-Gaussian wave height generated by Volterra series using a non-linear interaction matrix.

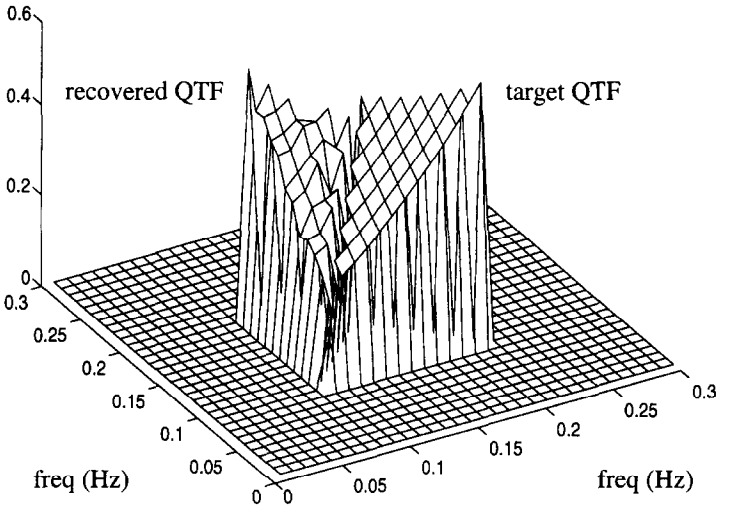

Fig. 13. Comparison of target QTF applied in Fig. 12, and the recovered QTF from a 1000 realization ensemble.

Table 3. Statistics of measured non-linear wave process and ensemble averaged simulated data

	Standard	Coefficient of skewness	Coefficient of kurtosis
Measured wave data	0.4950	2.2800	9.8329
Ensemble of 10 modified direct transformation simulations	0.3948	1.8911	8.5284
Ensemble of 10 neural network simulations	0.4692	2.1256	8.6640

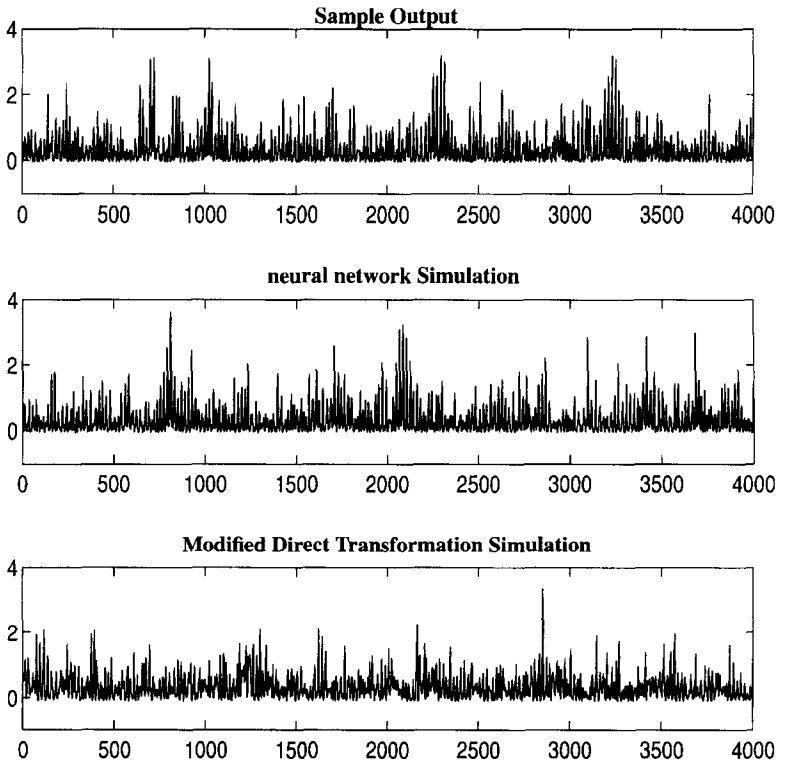

Fig. 14. Sample output from Gaussian sea state input using equation 16 (top), a simulation using a neural network trained on the sample input/output (middle), and a simulation using modified direct transformation.

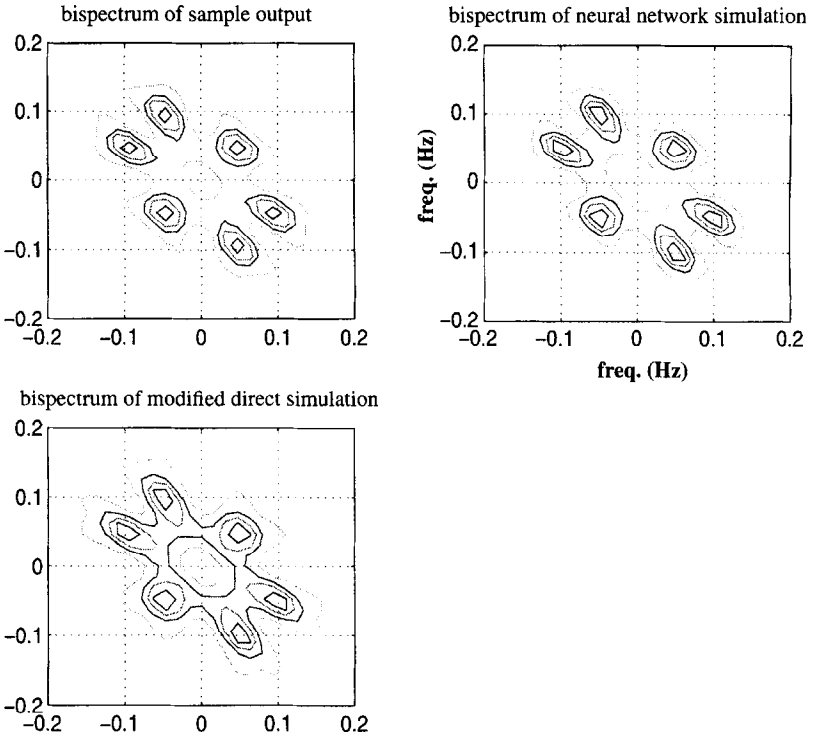

Fig. 15. Bispectrum contour of equation 16 output (top left), bispectrum contour of 10 neural network realizations (top right), and bispectrum contour of 10 modified direct transformation realizations.

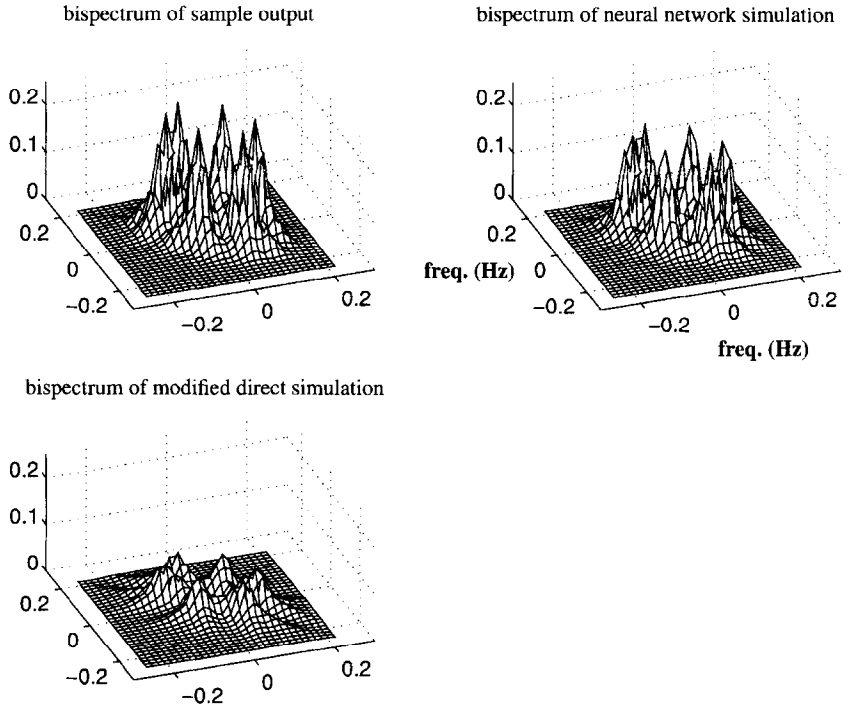

Fig. 16. Isometric view of Fig. 15. Bispectrum of equation 16 output (top left), bispectrum of 10 neural network realizations (top right), and bispectrum of 10 modified direct transformation realizations.

A neural network with two delays is trained to model the input/output from 4096 data points. This model is then used to simulate realizations of the output in equation (16) by passing Gaussian simulations of the input, η, through it. The modified direct transformation is also used to simulate the output directly, without knowledge of the input. A comparison

of statistical results is presented in Table 3, where it can be seen that the modified direct transformation does not match the statistics as well as in previous examples.

Figure 14 presents the original sample output in the top figure, and a neural network and modified direct transformation realization in the next two, respectively. The process being considered is a quadratic transformation of a Gaussian process. In order to demonstrate its non-Gaussian nature it is sufficient to consider the bispectrum. Figure 15 shows a contour representation of the bispectrum of the sample output process, and of an ensemble average of 10 realizations using the neural network and modified direct transformation models. At first glance, the modified direct transformation simulation bispectrum contour appears only slightly different from that of the neural network simulation and the sample, which are almost identical. However, the bispectrum from the modified direct transformation is significantly different, as seen in an isometric view of the bispectra in Fig. 16. This figure also shows the neural network bispectrum to closely resemble that of the original sample, due to the memory retention.

CONCLUSIONS

A class of non-normal processes are simulated based on information from the sample of a process. Static transformation techniques are applied to perform simulations of the underlying Gaussian time or autocorrelation sample. An optimization procedure is used to overcome errors associated with the truncation of static transformations. Several examples are presented to demonstrate the utility of this method. The inability of static transforms to retain the specific structure of the phase relationship between frequency components is addressed by the application of memory models. A Volterra series up to second order with analytical kernels is employed to simulate a non-Gaussian sea state. A neural network system identification model is utilized for simulation of output when system input is Gaussian wave elevation. This process is also simulated by the modified direct static transformation method using only the output sample process. It is demonstrated that the memory model is better able to achieve the shape and magnitude of the bispectrum of the original sample.

Acknowledgements—The support for this work was provided in part by ONR grant N00014-93-1-0761, and NSF grants CMS9402196 and CMS95-03779. The first and third authors were partially supported by a Department of Education GAANN Fellowship and a travel grant from the Institute of Engineering Mechanics, University of Innsbruck, during this study. Neural network software was developed by Ioannis Konstantopoulos under the guidance of Drs Nicos Makris and P. J. Antsaklis. Their cooperation is greatly appreciated.

REFERENCES

1. M. Shinozuka, Simulation of multivariate and multidimensional random processes. *J. Acoust. Soc. Am.* **49**, 357–368 (1971).
2. M. P. Mignolet and P. D. Spanos, Recursive simulation of stationary multivariate random processes. *J. Appl. Mech.* **54**, 674–687 (1987).
3. Y. Li and A. Kareem, Simulation of multivariate random processes: hybrid DFT and digital filtering approach. *J. Engng Mech. ASCE* **119**, 1078–1098 (1993).
4. T. T. Soong and M. Grigoriu, *Random Vibration of Mechanical and Structural Systems.* Prentice-Hall, Englewood Cliffs, NJ (1993).
5. M. K. Ochi, Non-Gaussian random processes in ocean engineering. *Prob. Engng Mech.* **1**, 28–39 (1986).
6. A. Kareem, K. Gurley and M. Tognarelli, Advanced analysis and simulation tools for wind engineering. *International Association for Wind Engineering, Proc. Ninth Int. Conf. Wind Engineering*, Vol. 5. Wiley Eastern, New Delhi (1995).
7. M. Grigoriu, Crossing of non-Gaussian translation process. *J. Engng Mech. ASCE* **110**(4), 610–620 (1984).
8. S. R. Winterstein, Nonlinear vibration models for extremes and fatigue. *J. Engng Mech. ASCE* **114**(10), 1772–1790 (1988).
9. R. N. Iyengar and O. R. Jaiswal, A new model for non-Gaussian random excitations. *Prob. Engng Mech.* **8**, 281–287 (1993).
10. R. Deutsch, *Nonlinear Transformations of Random Processes.* Prentice-Hall, Englewood Cliffs, NJ (1962).
11. D. Ammon, Approximation and generation of Gaussian and non-Gaussian stationary processes. *Struct. Safety* **8**, 153–160 (1990).
12. F. Yamazaki and M. Shinozuka, Digital generation of non-Gaussian stochastic fields. *J. Engng Mech. ASCE* **114**(7), 1183–1197 (1988).
13. M. Grigoriu, *Applied non-Gaussian Processes.* Prentice-Hall, Englewood Cliffs, NJ (1995).
14. D. A. Conner and J. L. Hammond, Modelling of stochastic system inputs having prescribed distribution and covariance functions. *Appl. Math. Modell.* **3**(2), 67–69 (1979).
15. G. E. Johnson, Constructions of particular random process. *Proc. IEEE* **82**(2), 270–285 (1994).

16. G. I. Schueller and C. G. Bucher, Non-Gaussian response of systems under dynamic excitation. In *Stochastic Structural Dynamics, Progress in Theory and Applications*, Ariaratnam, Schueller and Elishakoff (eds), pp. 219–239. Elsevier Applied Science, London (1988).
17. A. Kareem and Y. Li, On modelling the nonlinear relationship between random fields by means of higher-order spectra. In *Probabilistic Methods in Civil Engineering*, P. D. Spanos (ed.), pp. 384–387. ASCE, New York (1988).
18. P. D. Spanos and M. G. Donley, Equivalent statistical quadratization for nonlinear systems. *J. Engng Mech. ASCE* **117**(6), 1289–1309 (1991).
19. M. Schetzen, *The Volterra and Wiener Theories of Nonlinear Systems*. Wiley, New York (1980).
20. R. H. Peinelt and C. G. Bucher, Spectral analysis and synthesis of non-Gaussian processes. In *Structural Safety and Reliability*, G. I. Schueller, M. Shinozuka and J. P. Yao (eds), pp. 195–200. Balkema, Rotterdam (1994).
21. J. Zhao and A. Kareem, Response statistics of tension leg platforms under wind and wave loads: a statistical quadratization approach. *ICOSSAR*, Austria (1993).
22. A. Kareem and J. Zhao, Stochastic response analysis of tension leg platforms: a statistical quadratization and cubicization approach. In *Proc OMAE '94 Conf.*, Vol. 1. ASME, New York (1994).
23. S. W. Nam, E. J. Powers and S. B. Kim, Applications of digital polyspectral analysis of non-linear system identification. In *Proc. 2nd IASTED Int. Symp. Signal Processing and its Applications*, Gold Coast, Australia, pp. 133–136 (1990).
24. S. A. Billings and K. M. Tsang, Spectral analysis for non-linear systems, Part I: parametric non-linear spectral analysis. *Mech. Systems Signal Process.* **3**(4), 319–339 (1989).
25. J. S. Bendat and A. G. Piersol, *Random Data Analysis and Measurement Procedures*. Wiley, New York (1986).
26. M. Wright and J. K. Hammond, The convergence of volterra series solutions to nonlinear differential equations. In *Structural Dynamics: Recent Advances. Proc. 4th Int. Conf.*, M. Petyt, H. F. Wolfe and C. Mei (eds), pp. 422–431. Elsevier Applied Science, London (1990).
27. I. J. Leontaritis and S. A. Billings, Input–Output parametric models for non-linear systems, Part I: deterministic non-linear systems. *Int. J. Control* **41**(2), 303–328 (1985).
28. S. Chen, S. A. Billings and W. Luo, Orthogonal least squares methods and their application to non-linear system identification. *Int. J. Control* **50**(5), 1873–1896 (1989).
29. S. Y. Kung, *Digital Neural Networks*. Prentice-Hall, Englewood Cliffs, NJ (1993).
30. R. T. Hudspeth and M. C. Chen, Digital simulation of nonlinear random waves. *J. Waterways Port Coastal Ocean Div. ASCE* **105**, 67–85 (1979).
31. K. Hasselmann, On the nonlinear energy transfer in a gravity wave spectrum, Part I. *J. Fluid Mech.* **12**, 481–500 (1962).
32. L. J. Tick, Nonlinear probability models of ocean waves. In *Ocean Wave Spectra*, pp. 163–169. Prentice-Hall, Englewood Cliffs, NJ (1963).
33. A. Kareem and Hsieh, Probabilistic dynamic response of offshore platforms to wave loads. *Technical Report no. NDCE91-1*, Department of Civil Engineering, University of Notre Dame (1991).